Power System Technology **Volume 45 · Number 2 · 2021**
ISSN: 1000-3673

Modeling of Thermoelectric Generator for Powering Wireless Temperature Sensor Node Employed in Condition Monitoring System of HVDC Converter

Lan T., Lan Y., Sheng C., Liu W., He Q., Yang H., Liu Y.
Computational Mechanics Group, Department of Mechanical Engineering, School of Mechanical and Manufacturing Engineering, National University of Sciences and Engineering, China

ABSTRACT

This study revolves around the ballistic response of Al_2O_3/Al 5083-H116 bi-layer armour against a 12.7 mm Armour Piercing (AP) tracer projectile. The study features the experimental and numerical study where the penetration of the AP projectile through a semi-infinite Al 5083-H116 target and Al_2O_3/Al 5083-H116 armour were determined. The semi-infinite Al 5083-H116 target consisted of three aluminium plates where the projectiles penetrated the first two plates. On the other hand, the bi-layer Al_2O_3/Al 5083-H116 armour arrested the armour piercing projectile after it penetrated the ceramic plate. A FEA model was also developed to investigate the impact phenomenon and predict the depth of penetration. High strain-rate deformation of ceramic material was modelled with Johnson Holmquist damage model for ceramics (JH-2), and that of the Al 5083-H116 was modelled with Johnson-Cook material model. During the impact simulation the progressive failure of the AP tracer projectile was observed. The predicted residual penetration depth and the hole size in the ceramic plate were lower than the experimentally observed values. The ballistic efficiency factor of the Al_2O_3/Al 5083-H116 bi-layer armour was higher than one showing that the bi-layer armour was better in terms of mass efficiency and space efficiency in comparison to Al 5083-H116 armour.

1. INTRODUCTION

Ceramics have lower density and higher compressive strength than steels that makes them more suited as protection against armour piercing projectiles. During the impact, the tip of the projectile is broken by a ceramic front plate and a back plate of ductile material absorbs the impact of the fractured AP projectile and thus completely stops the projectile. Ceramic materials usually used in armour systems include Alumina (Al_2O_3, Silicon-Carbide (SiC) and Boron-Carbide (B_4C). The ballistic performance of ceramic armours can be evaluated by determining the ballistic performance measure. Relative performance measures are used to compare the performance of different penetrators and material combination.

Such measures are generally based on the comparison of an intrinsic property of the armour protection system such as mass, thickness, penetration depth, etc. where a reference armour system is brought in comparison with the performance of the armour system. Depth of penetration (DOP) based performance measure was suggested by Rosenberg et al. [1] where a ceramic tile is stacked against a thick metal back plate. The DOP measure provides equivalent performance of ceramic compared to a semi-infinite metal plate, which is commonly Rolled Homogenous Armour (RHA). Space and mass efficiencies were defined by Frank [2] as dimensionless measures of ballistic performance of an armour system and are defined as;

$$E_s = {t_0}/{t} \tag{1}$$

$$E_m = {\rho_0 . t_0}/{\rho . t} \tag{2}$$

Here, t_0 and ρ_0 refer to the thickness and density of the reference armour steel that stopped the projectile from further penetrating. Whereas t and ρ are the thickness and density of material to be evaluated. These efficiencies include terms for the difference between the penetration depth in a reference semi-infinite material and the residual depth in a back plate used with a ceramic plate. Product of the mass and space efficiencies was defined as ballistic performance factor that gives an overall measure of the performance. Mass and space efficiency values of higher than one indicates a better performance compared to the reference material. A differential efficiency factor (DEF) was defined by Yaziv et al. [3] that is based on areal density and penetration depths.

Ballistic performance of an Alumina / Aluminium 603 armour steel impacted by tungsten rods was experimentally and numerically investigated by Jinzhu et al. [4]. They reported a linear relationship in between the depth of penetration (DOP) in between the steel back plate and ceramic thickness. The mass and the differential efficiency factors increased as the ceramic thickness was increased. Experimental investigation on 95% and 99.5% alumina tiles ballistic response against 12.7 mm AP projectile was carried out by Madhu et al. [5]. A ballistic efficiency factor (BEF) based on the work of Frank [2] was calculated that varied as a function of ceramic thickness and the projectile velocity. Alumina 99.5% had higher ballistic performance than alumina 95%. However, the ballistic efficiency factor of alumina 99.5% decreased as the thickness increased and BEF increased with increasing thickness for alumina 95%. An increase in differential efficiency factor (DEF) with an increase in the projectile velocity was reported by Savio et al. [6] when boron carbide (B4C) tiles were impacted by 7.62mm AP Projectile. Rosenberg et al. [1] performed impact tests on alumina tiles (AD 85) of varied thickness by firing AP projectiles of 0.3”, 0.5” and 14.5 mm. The residual penetration and the ceramic tile thickness had a linera relationship for all types of AP projectiles. It has been argued by Rosenberg and Dekel [7] that the experimental results showing a linear relationship between the residual penetration and ceramic tile thickness for various projectiles show that ballistic efficiency is independent of tile thickness. The inconsistencies in various results reported in the literature are attributed to the difficulties in the reproduction of ceramic tiles with consistent material properties and the effects related with thick or thin tiles. Thus, selection of tile thickness was considered important for determining the ballistic efficiency.

It was reported by Wang et.al [8] that the formation of hole diameter, crater depth and penetration depth were dependant on the design of shaped charge. Numerical simulations based on finite element modelling provide a tool feasible for the study of the high-speed impact. In most of the numerical studies, the ceramic material definition is generally based on the Johnson-Holmquist material models; JH-1 and JH-2 [9, 10]. The Johnson-Holmquist models are phenomenological material models that predict the strength and failure of a ceramic. JH-1 material model predicts the failure of material instantaneously whereas JH-2 material model can predict damage in material. Pawar et al. [11] compared the ballistic performance of Al_2O_3/Al 5083 and A1N/Al 5083 ceramic armours by finite element method. The ceramic materials were defined using JH-2 material model. 7.62 mm AP bullets were impacted on the armour, and it was reported that the ballistic performance of AIN/Al 5083 was superior to Al_2O_3/Al 5083. Venkatesan et al. [12] compared the ballistic performance of SiC/Al with Al_2O_3/Al armour numerically. JH-2 material model was used for both ceramics, and it was reported that the high compressive strength of the SiC ceramic caused more damage to the projectile. Thus, SiC/Al ceramic had better ballistic performance than Al_2O_3/Al ceramic. It can be seen that JH-2 based finite element simulations of various types of ceramic materials were successful in predicting the material behaviour under ballistic conditions.

The current study is based on a DOP experimental testing of Alumina 95 and Al 5083-H116 bi-layer armour. 12.7 mm AP tracer projectiles are impacted on the bi-layer armour. DOP in a semi-infinite target of Al 5083-H116 is determined and used as a reference penetration depth for ballistic performance determination of the Al_2O_3/ Al 5083-H116 armour. Finite element models of the semi-infinite Al 5083-H116, and Al_2O_3/ Al 5083-H116 bi-layer armour plates are developed. The DOP, deformation of the ceramic and the aluminium material, hole formation, and the failure predicted by the FE model are compared with the results gathered from experimentation. Moreover, the underlying failure mechanisms of the ballistic efficiency of the Al_2O_3/ Al 5083-H116 armour are discussed.

2. EXPERIMENTATION

The study also featured experimentation to obtain the ballistic response by the ceramic plate when it was impacted by a 12.7 mm AP tracer projectile. Ceramic plate had hexagonal ceramic tiles bonded together, and a thin aluminium sheet was placed at front and back of the hexagons. X-Ray diffraction of ceramic material performed on an XRD powder diffraction system by STOE & Cie GmbH, Germany revealed alumina 95% as the ceramic material. Results of XRD analysis are shown in Figure 1. Micro-hardness testing gave an average hardness of 1270 HV. The ceramic plate was 500 x 500 x 13.5 mm in size. Ceramics are brittle and fracture easily under impact, thus, a ductile back plate of aluminium 5083-H116 was included in the setup. Aluminium 5083-H116 is an aluminium-magnesium alloy. It is a high strength Al-Mg alloy and finds its uses in protective structures and marine applications. Mechanical properties of aluminium 5083-H116 are provided in Table 1. The Aluminium back plate was 800 x 800 x 38.1 mm in size.

The 12.7 mm AP tracer projectiles impacted the combination of the ceramic and back plate. AP projectile has a hardened steel core. In tracer bullets, core part is hollow which is filled with pyrotechnic charge which burns brightly when it impacts the target. Such projectiles find application in tracking the trajectory of the projectile or designating targets. The outer jacket is made up of brass. The projectile and its dimensions are shown in Figure 2.

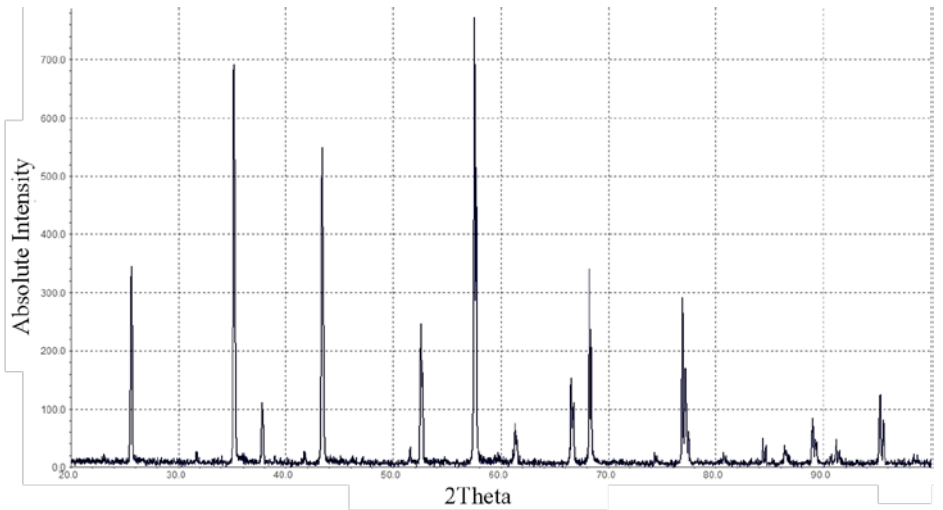

Figure 1: Results of XRD analysis of the ceramic plate.

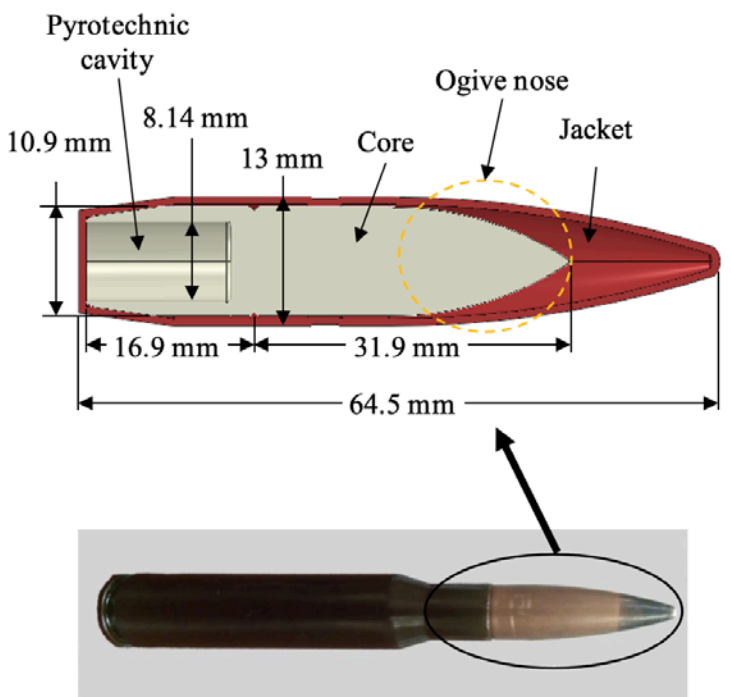

Figure 2: Cross-sectional view of the 12.7 mm AP tracer projectile revealing the core and the pyrotechnic cavity.

Experiments were performed in two stages. Initially, a semi-infinite target was created by stacking three aluminium back plates, and three projectiles were fired. A semi-infinite target allowed determination of the penetration depth of the 12.7 mm AP tracer projectile in Aluminium 5083-H116. The back plates were mounted on a stand where they were held in place using a fixture and were at a distance of 300 m from the projectile firing point. The velocity was measured by a Super Chrono acoustic chronograph manufactured by Steinert Sensing Systems, Norway. The distance in between chronograph and the point of firing the projectile was two meters. Later, the ceramic plate was placed in front of the back plates the 12.7 mm AP tracer projectiles were fired. The average recorded velocity of the projectiles was 864 m/s with a variation between 850-882 m/s. Schematic representation of the experimental setup is shown in Figure 3 and the target plates mounted in the fixture are shown in Figure 4.

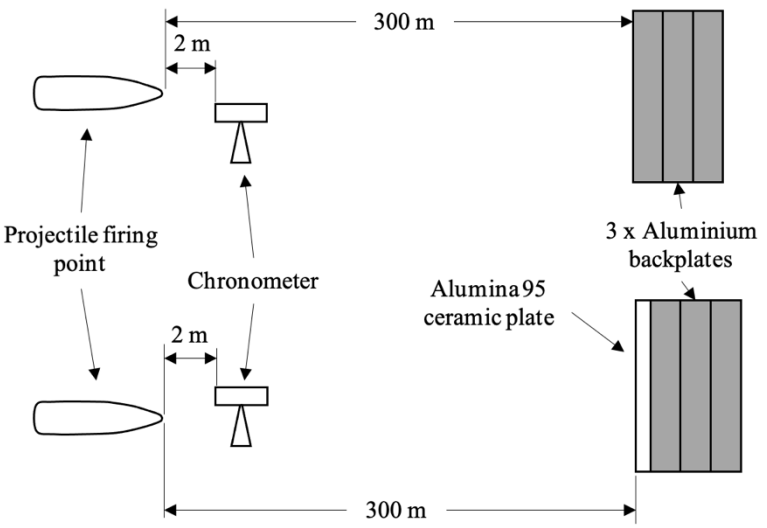

Figure 3: Schematic representation of the experimental setups (a) semi-infinite aluminium 5083-H116 backup plates (b) ceramic plate with backup plates (not to scale).

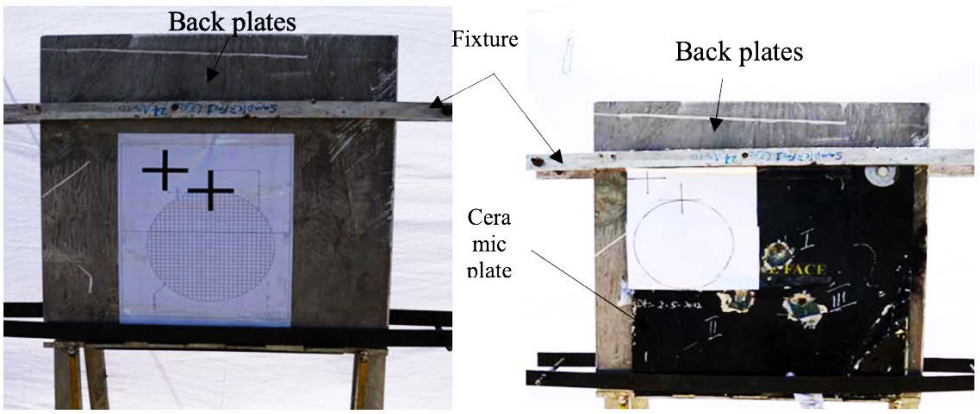

Figure 4: Mounting of target plates in the fixture (a) back plates (b) ceramic and back plates.

Table 1: Mechanical properties of aluminium AA5083-H116 [27].

Elastic Modulus (GPa)	Shear Modulus (GPa)	Yield Strength (MPa)	Ultimate Tensile Strength (MPa)
70.3	26.4	320	315

3. FINITE ELEMENT MODELLING

The experimental setup was replicated by creating a Finite Element model with the commercial finite element code Abaqus/Explicit which is developed by Dassault Systemes. Separate finite element models were set up for the semi-infinite aluminium target plates and the ceramic with aluminium back plates. Due to the symmetry in geometry, loading and boundary conditions, only one-quarter geometry was modelled. A plate having a 150 x 150 mm size was modelled for ceramic and aluminium back plates, as the deformation and fracture because of the projectile impact are highly localised. The semi-infinite aluminium plate model consisted of three aluminium back plates of 38.1 mm thickness stacked against each other, while the ceramic plate model included the ceramic plate stacked against a single aluminium back plate to conserve the computational resources. The 12.7 mm AP tracer projectile model featured two different parts; core and the jacket. The core section having pyrotechnic charge was not included in the simulation as the core ricochets upon impact with the target [13]. The initial configurations of the two finite element models are shown in Figure 5.

The mesh type was eight node continuum hexahedral elements with reduced integration formulation (C3D8R) for ceramic and the back plate. Reduced integration are preferred under contact conditions and also provide better computational performance [14] . The region of impact was discretised using the smallest element size and using the biased seeds the element size was increased for regains away from impact point. Aluminium back plates were discretised with the smallest element size of 0.8 x 0.8 x 0.5 mm while the ceramic plate had a minimum element size of 0.5 x 0.5 x 0.5mm.

Convergence of residual velocity and penetration depth determined the minimum mesh sizes. A combination of “eight node continuum hexahedral reduced integration elements” (C3D8R) and “six node continuum wedge reduced integration elements” (C3D6R) having a minimum mesh size of 0.5 x 0.5 x 0.5mm was used for projectile core. Only ogive nose of the core had continuum wedge elements to generate a mesh with minimal initial distortion. The finite element meshes can be seen in Figure 5.

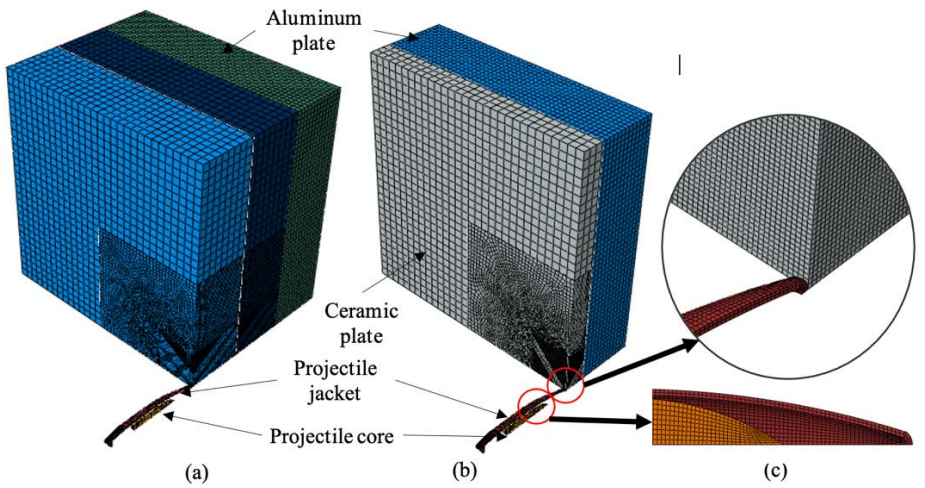

Figure 5: Initial configuration and meshing of the simulation models (a) semi-infinite aluminium plates (b) ceramic plate with a single aluminium back plate (c) a zoomed-in view of the fine meshed region.

The ceramic plate and the back plates were fully constrained at edges. Boundary Conditions for symmetry were applied on appropriate faces of the plates, the core and the jacket as shown in Figure 6. The initial velocity of 864 m/s was provided to the projectile core and the jacket. Penalty based friction formulation was used with a friction coefficient of 0.08 [15] for semi-infinite aluminium plate model while the ceramic plate model had a friction coefficient of 0.35 [16]. Contact surface definition also had included the interior elements of the projectile jacket and the base armour plate meshes due to surface erosion during the impact. The aluminium sheets used as covering of the ceramic plate were not included in simulations as their effect on ballistic performance of the ceramic plate is considered negligible.

Material behaves hydrodynamically during impact and can be modelled using Mie-Grüneisen equation of state (EOS). Mie-Grüneisen EOS gives a linear relationship in between particle velocity and shock velocity. The general form of the Mie-Grüneisen EOS is provided as:

$$P = P_{ref} + \Gamma\rho\,(I - I_{ref}) \tag{1}$$

here P represents the pressure, P_{ref} represents the reference pressure, density is represented by ρ, specific internal energy is denoted by I and Γ represents the Grüneisen parameter which is considered a function of volume. A fit to the Hugoniot data may be obtained by plotting the experimental data in the plane of particle and shock velocity [17]. The linear equation representing the fit to experimental data is given by Equation (2)

$$U = C + S.u \tag{2}$$

where C is bulk sound speed and U have units of velocity. Also, P_{ref} can be calculated from Equation (3)

$$P_{ref} = \frac{\rho_0 C^2 \eta}{(1-S\eta)^2} \tag{3}$$

where ρ_0 is the reference density and $\eta = 1 - {}^{\rho_0}/_{p}$. Mie-Grüneisen EOS was added in the material model of the steel core, the brass jacket and aluminium back plate and parameters of EOS for those materials are given in Table 2.

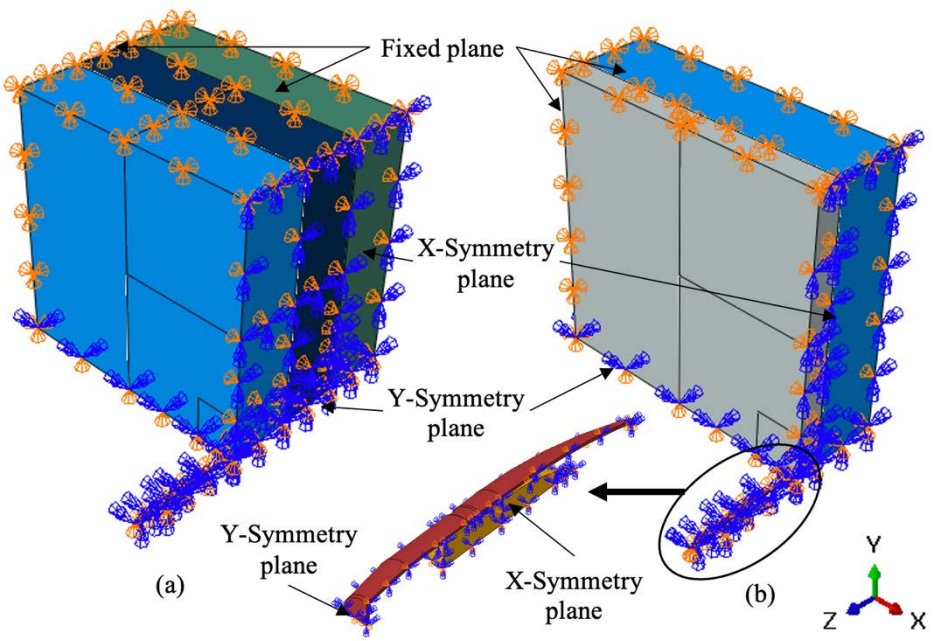

Figure 6: Boundary conditions applied to the finite element models (a) semi-infinite aluminium plates (b) ceramic plate with a single aluminium back plate.

Table 2: Mie-Grüneisen equation of state parameters.

Parameter	Symbol	Unit	Al 5083-H116 [28]	Projectile Core [29]	Brass [29]
Elastic wave velocity	C	m/s	5340	4570	3940
Slope values	S	-	1.4	1.49	1.49
Grüneisen parameter	Γ	-	1.97	1.93	1.99

Plastic deformation of the aluminium back plate, the Johnson-Cook plasticity model [18] was basis for projectile core and the jacket; that provides flow stress based on strain, strain rate and adiabatic heating. J-C plasticity model has been widely used for high strain applications [19-21]. General form of the Johnson-Cook plasticity model is given in Equation (4) [17] as:

$$\sigma = [A + B\varepsilon^n][1 + C\, ln\, \dot{\varepsilon}^*][1 - (T^*)^m] \tag{4}$$

here A, B, C, m and n refer to experimentally determined material parameters. The non-dimensional temperature T* is determined by Equation (5).

$$T^* = \frac{(T - T_{ref})}{(T_{melt} - T_{ref})} \tag{5}$$

here T_{ref} refers to the temperature below which the material does not show any temperature dependence on flow stress and T_{melt} is the melting temperature. Equation (6) provides the relation for strain rate [17].

$$\dot{\varepsilon}^* = \frac{\dot{\varepsilon}}{\dot{\varepsilon}_0} \tag{6}$$

where $\dot{\varepsilon}^*$ is the dimensionless strain rate, $\dot{\varepsilon}_0$ is the reference strain rate and $\dot{\varepsilon}$ is the equivalent strain rate.

Johnson Cook (JC) plasticity model parameters are given in Table 3. Failure and damage of core and metal back plate were defined by Johnson-Cook damage material model [17]. The initiation of damage is determined by Equation (7), which gives the equivalent plastic strain at the onset of damage.

$$\varepsilon^{pl} = \left[d_1 + d_2 e^{(-d_3 \eta)}\right]\left[1 + d_4\, ln\left(\frac{\dot{\varepsilon}^{pl}}{\dot{\varepsilon}_0}\right)\right](1 + d_5 T^*) \tag{7}$$

where d_1, d_2, d_3, d_4 and d_5 are material parameters and η is pressure-deviatoric stress ratio. $\dot{\varepsilon}_0$ represents the reference strain rate. Also D is used for defining the accumulative material

damage where the value of D varies in between 0 and 1. Here 0 refers to a material without any damage while 1 refers to a fully damaged material. Once $D = 1$, material failure occurs and respective elements were removed from the FEA model. Parameters for J-C (Johnson Cook) damage model in Table 4. It is worth noting that in the previous work [22], erosion of the AP projectile nose after penetration of 38.1mm thick aluminium plate was not observed during the experimentation. Thus, a failure displacement of 0.4 was used for the projectile ogive nose elements to reduce the erosion during the penetration of the aluminium plates. The brass jacket failure was determined based on a critical fracture strain $\varepsilon_f = 0.4$[23].

The response of ceramic material (Alumina-95) was based on JH-2 (Johnson Holmquist) material model. The JH-2 material model considers that plastic deformation causes damage in a material and damage increases with increasing plastic deformation. It consists of an equation of state (EOS) for determining the pressure, a strength model that determines the strength of the material when in intact and fractured states and a damage model that is based on plastic strain. The pressure-density relationship is based on an EOS given by Eq. (8) [14].

$$\begin{aligned} P &= K_1.\mu + K_2.\mu^2 + K_3.\mu^3 \quad \text{if} \quad \mu \geq 0, \\ P &= K_1.\mu \quad \text{if} \quad \mu \leq 0 \end{aligned} \tag{8}$$

where K_1 represents bulk modulus and K_2, K_3 are EOS constants. The parameter μ is given by $\mu = \rho/\rho_0 - 1$ where ρ is current density and ρ_0 is initial density.
Strengths have been normalised in JH-2 material model and strength of the material in terms of normalised von Mises stress is given by Eq. (9) [14].

$$\sigma^* = \sigma_i^* - D\left(\sigma_i^* - \sigma_f^*\right) \tag{9}$$

where σ^* is the normalised intact equivalent stress, σ_i^* is the normalised fracture equivalent stress and D is the damage variable. The normalised stresses are obtained by normalising the actual equivalent stress to the equivalent stress as Hugoniot Elastic Limit (HEL). The normalised intact strength is given by Eq. (10) [14].

$$\sigma_i^* = A.(P^* + T^*)^N(1 + C\ ln\dot{\varepsilon}^*) \tag{10}$$

and the fractured strength is stated by Eq. (11) as [14]:

$$\sigma_f^* = B.(P^*)^M\ (1 + C\ ln\dot{\varepsilon}^*) \tag{11}$$

where A, B, C, M and N are the material constants, P^* is normalised pressure and T^* is normalised maximum tensile pressure. Pressures are normalised to the pressure at HEL.

Damage in the material is represented by a single parameter D that is given by Eq. (12) [24].

$$D = \sum \frac{\Delta \varepsilon^P}{\varepsilon_f^P} \tag{12}$$

where $\Delta \varepsilon^P$ is the incremental plastic deformation and ε_f^P is given by Eq. (13) [24].

$$\varepsilon_f^p = D_1 \left(P^* + T^* \right)^{D_2} \tag{13}$$

where D_1 represents damage coefficient and D_2 is damage exponent. Erosion of the ceramic plate due to projectile penetration was based on a failure strain (FS) criterion with FS = 2.0. Failure strain values of 1.5 to 3.0 have been used in literature [25, 26]. The JH-2 parameters for alumina-95 are mentioned in Table 5.

Table 3: Material parameters for the projectile and the back plate.

Parameter	**Symbol**	**Unit**	**Al 5083-H116 [19]**	**Projectile Core [30]**	**Brass [23]**
Density	ρ	kg/m^3	2700 [20]	7850	8960 [29]
Shear Modulus	G	GPa	26.4 [27]	76.9	46 [29]
Specific heat	C_p	J/kg.K	910 [20]	455	386
Johnson-Cook Plasticity Model Parameters					
Initial yield stress	A	MPa	167	1657.71	90
Strain hardening coefficient	B	MPa	596	20855.6	628.03
Strain hardening exponent	n	-	0.551	0.651	0.7201
Thermal softening exponent	m	-	0.859	0.35	1
Melting Temperature	T_{melt}	K	893	1800	1288
Reference Temperature	T_{ref}	K	293	293	294
Strain rate coefficient	C	-	0.001	0.0076	0.2659
Reference strain rate	ε_0^*	1/s	1	1	745.82

Table 4: Johnson-Cook damage model parameters.

Material	d_1	d_2	d_3	d_4	d_5
Al 5083-H116 [19]	0.0261	0.263	-0.349	0.147	16.8
Projectile Core [30]	0.0301	0.0142	-2.192	0.0	0.35

Table 5: Parameters of the JH-2 material model for alumina 95 [31].

Density, $\rho_0(\mathrm{kg/m^3})$	3741
Bulk Modulus, $K_1(\mathrm{GPa})$	184.56
EOS Constant, $K_2(\mathrm{GPa})$	185.87
EOS Constant, $K_3(\mathrm{GPa})$	157.54
Shear Modulus, $G(\mathrm{GPa})$	120.34
Hugoniot Elastic Limit (HEL) (GPa)	6
Strength Constant, A	0.889
Strength Constant, N	0.764
Strain Rate Constant, C	0.0045
Strength Constant, B	0.29
Strength Constant, M	0.53
Normalised Maximum Fracture Strength, σ_f^{max}	1
Damage Constant, D_1	0.005
Damage Constant, D_2	1
Bulking Factor, β	1
Pressure at HEL, $P_{HEL}(\mathrm{GPa})$	3.26

4. RESULTS AND DISCUSSION

Initial experiments were carried out to obtain the penetration depth of the 12.7 mm tracer AP projectile in aluminium 5083-H116 back plates, and three plates were stacked to make a semi-infinite target. The penetration of the projectile in the semi-infinite target is shown in Figure 7 where a lip formation can be seen upon entry of the projectile in the first back plate. The projectile penetrated the first and second back plates and was stopped by the third back plate. The exit holes in the second back plate can also be seen in Figure 7. The average DOP was 76.46±5.2 mm.

The material failure was localized and the phenomenon of ductile hole growth was observed that pushes the material in the plate aside and creates a passage for the penetrating projectile. Formation of lips on the exit holes of the second back plate was suppressed because of the presence of the third back plate. The semi-infinite target had no localised bending. The hole formed in the ceramic plate after penetration of the projectile is shown in Figure 8. The fracture of the ceramic was brittle, and the damage and failure in the ceramic material were localised. The thin aluminium sheets at the front and back of the ceramic material deformed by forming curved petals. The projectile penetrated the ceramic plate completely. However, the ceramic plate owing to brittle fracture absorbed most of the energy of 12.7 mm tracer AP projectile. The ceramic plate also makes the projectile blunt, and thus it becomes unable to penetrate even the first aluminium back plate and a crater with average depth of 11.52±1.1 mm was formed in the first back plate.

Figure 7: Holes caused by the penetration of the 12.7 mm AP tracer projectile in semi-infinite aluminium back plates (a) impact side of the first back plate (b) exit side of the second back plate.

Finite element models for the semi-infinite aluminium plates, and ceramic plate with a single back plate were used to predict the penetration and ballistic response of the 12.7mm AP tracer Projectile. When the projectile impacted the semi-infinite aluminium plate, the projectile jacket makes the first contact and progressively fractures before the hardened projectile core starts penetrating the aluminium plates. The failure of the core ogive nose is shown in Figure 9. The projectile core penetrated the first and second aluminium plates, and ductile hole growth occurred where a penetration depth of 71 mm was predicted which is only ~ 7.7% less than the experimentally observed average penetration depth. Figure 10 shows the penetration of 12.7 mm tracer AP projectile through the aluminium plates.

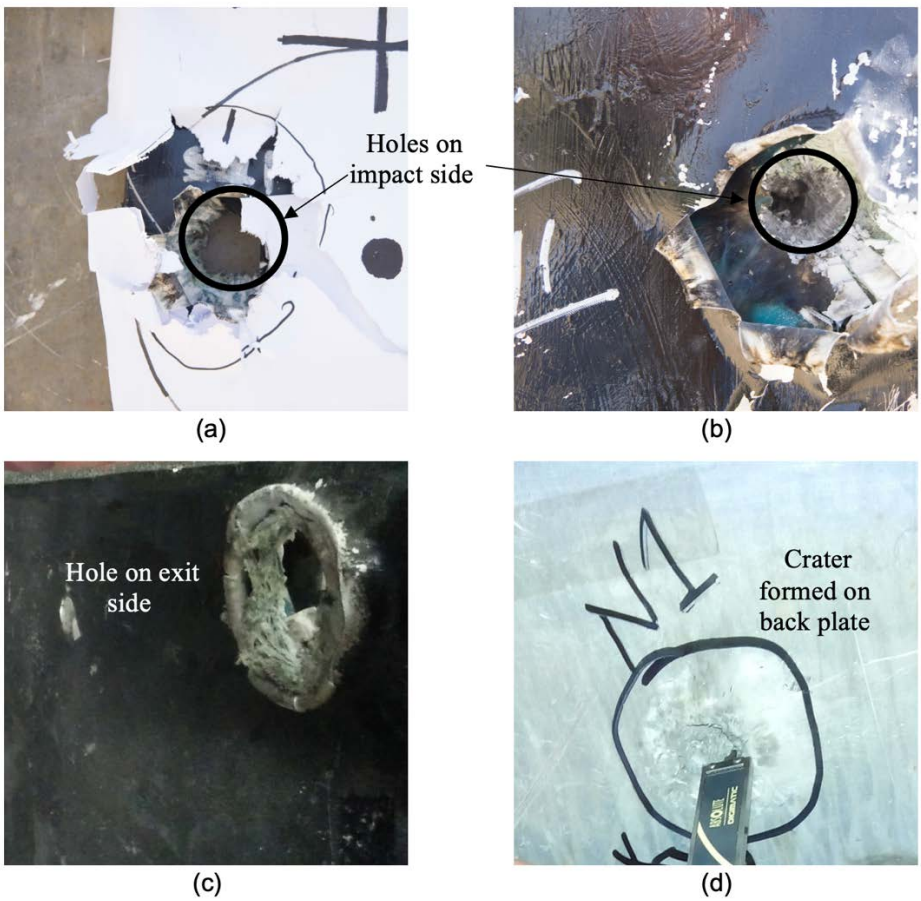

Figure 8: Resulting holes after penetration of the projectile in ceramic target plate and crater formed on the back plate.

In the second setup the projectile impacted the ceramic plate with a single aluminium back plate. Progressive erosion of the projectile core occurs during the penetration process that completes after complete penetration through the ceramic plate and by creating a crater in the back plate. Penetration of 12.7 mm tracer AP Projectile through the ceramic and back plate can be seen in Figure 11. The ceramic plate fractures the projectile tip and blunts the projectile during the impact while absorbing the projectile energy by self-fracture. The back plate deforms plastically as it absorbs the remaining projectile energy once it penetrates the ceramic plate. The equivalent plastic strain contours in the back plate are shown in Figure 12 where the localized plastic strain develops at the interface of the Alumina plate and the Aluminium back plate. The finite element model predicted a crater depth of 7.2 mm which is more conservative than the experimentally observed results.

The average hole diameter in the ceramic plate was predicted to be 14.8 mm as opposed to the experimentally observed average hole diameter of 17.03±1.72 mm. This can be related to the differences between the experimental setup and an ideal case depiction by Johnson Holmquist (JH-2) Damage Model parameters taken from the literature. Since the material deformation is brittle, no lip formation was observed in the simulation model. Figure 13 shows the hole as predicted by the FEA model and the holes resulting after experimentation in the ceramic plate.

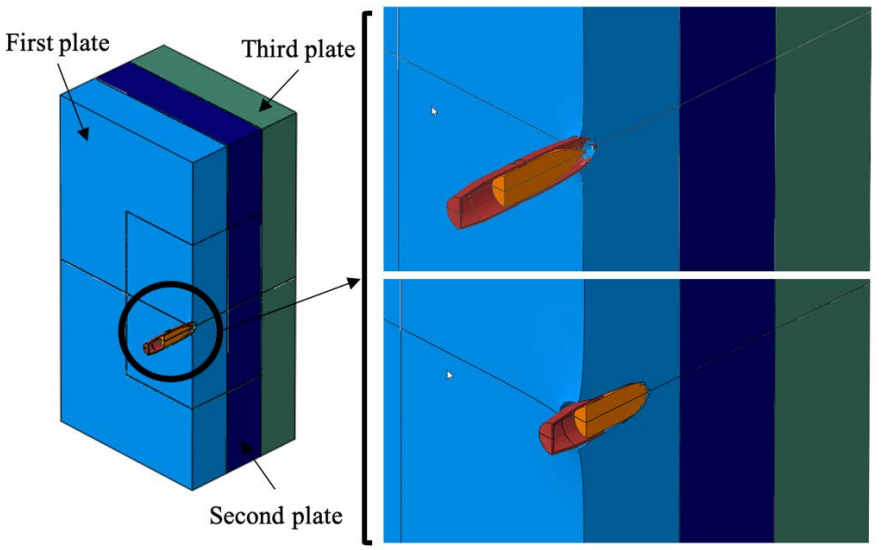

Figure 9: Failure of jacket upon impact with the semi-infinite aluminium target plate.

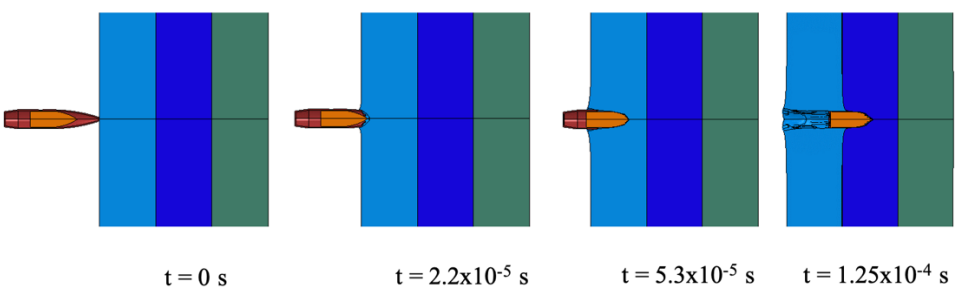

Figure 10: Progression of the projectile through the Aluminium Plates

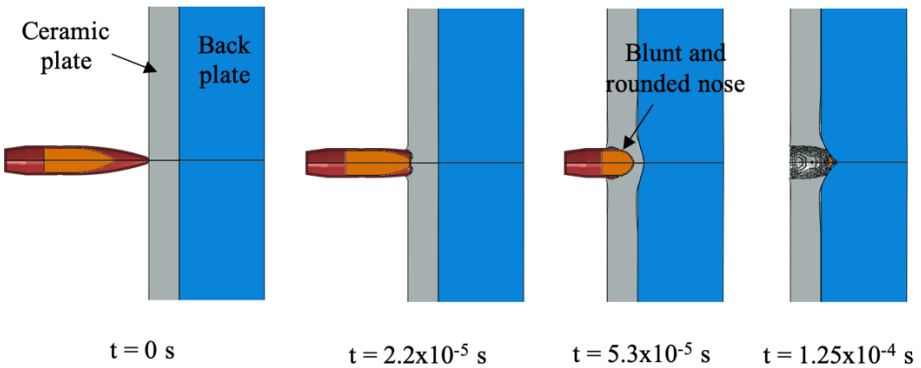

Figure 11: Progression of the projectile through the ceramic and back plate.

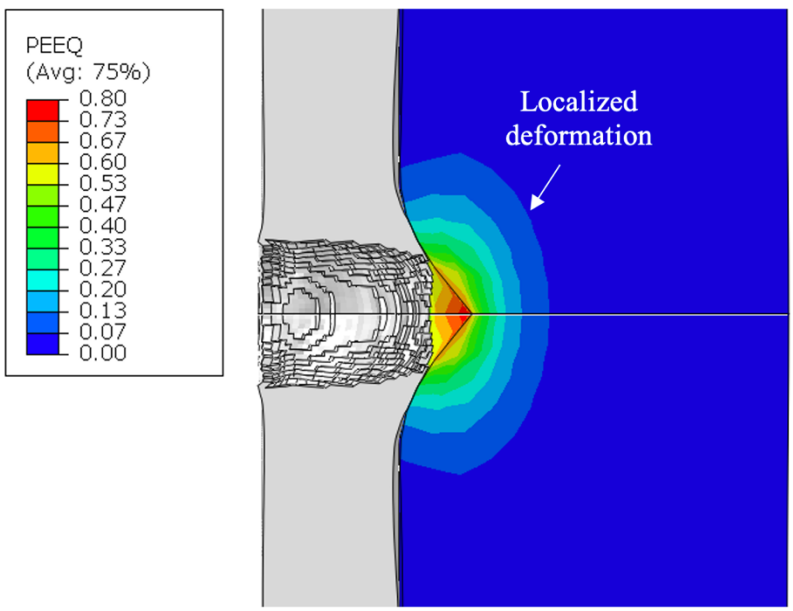

Figure 12: Equivalent plastic strain developed in the back plate after projectile impact.

A dimensionless ballistic efficiency factor can be calculated to compare the performance of the semi-infinite aluminium plate armour, and ceramic with aluminium back plate armour. This factor includes mass and thickness efficiencies of the armour. The semi-infinite aluminium plate armour is considered as the reference armour system in this case and thickness and mass efficiencies of the ceramic with single back plate armour were calculated using Eq. (14) and (15) [5].

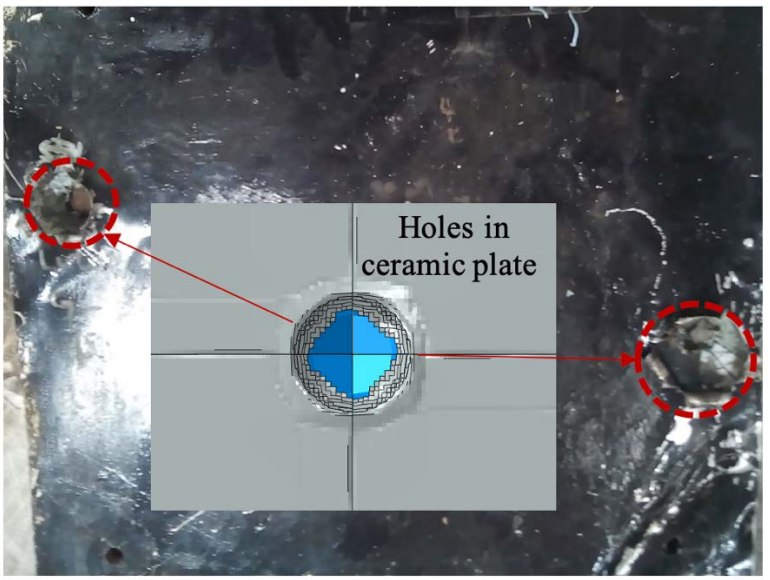

Figure 13: Hole after penetration of 12.7 mm AP tracer bullet in the ceramic plate as predicted by the finite element method and observed experimentally

$$E_t = \frac{P_{reference} - P_{res}}{t_{ceramic}} \tag{14}$$

$$E_m = E_t \times \frac{\rho_{reference}}{\rho_{ceramic}} \tag{15}$$

where P_{ref} is the penetration depth in the reference armour system, P_{res} is the depth penetrated by the projectile in the back plate when used with the ceramic plate, $t_{ceramic}$ is the thickness of the ceramic plate, ρ_{ref} is the density of the reference armour system and $\rho_{ceramic}$ is the density of the ceramic (alumina) plate. The Ballistic Efficiency Factor (BEF) was calculated by Eq. [5].

$$q^2 = E_t \times E_m \tag{16}$$

For the ceramic and single back plate armour system under discussion, $q^2 = 16.7$ with $E_t = 4.81$ and $E_m = 3.47$. E_t and E_m values are higher than 1.0 showing that the ceramic and back plate armour is thinner and lighter than the equivalent semi-infinite aluminium plate armour. Such factors can be used during design to evaluate the comparative performance of available armours.

5. CONCLUSIONS

The study undertook a bi-layer Al_2O_3/Al 5083-H116 armour against 12.7 mm AP tracer projectile and investigated the phenomenon experimentally as well as through numerical model. The DOP of the 12.7 mm tracer AP projectile in semi-infinite Al plate was determined as reference residual depth and was used to determine the ballistic efficiency of the bi-layer Al_2O_3/Al 5083-H116 armour. Upon impact with the Al_2O_3/Al 5083-H116 armour, the projectile progressively failed. The ceramic plate blunted the tip of the projectile core that was stopped by the ductile back plate. The back plate deformed plastically at the location of the impact. The numerical simulation successfully predicted the general characteristics like DOP and the hole diameter. The difference between the FEA simulations and experimental results may be attributed to the material model parameters that were taken from the literature. The ballistic efficiency of the Al_2O_3/Al 5083-H116 armour was higher than that of an all-aluminium armour and thus may be used effectively to protect against 12.7 mm AP tracer projectiles.

REFERENCES

[1] Rosenberg, Z., et al. "A new definition of ballistic efficiency of brittle materials based on the use of thick backing plates." DGM Informationsgesellschaft mbH, Impact Loading and Dynamic Behavior of Materials. 1 (1988): 491-498.

[2] K. Frank, Armor-penetrator performance measures. ARBRL, 1981

[3] D. Yaziv, G. Rosenberg, Y. Partom, Differential ballistic efficiency of appliqué armor, 10th international symposium on ballistics. Shrivenham, UK, 1986 pp. 315-319

[4] L. Jinzhu, Z. Liansheng, H. Fenglei, Experiments and simulations of tungsten alloy rods penetrating into alumina ceramic/603 armor steel composite targets, International Journal of Impact Engineering. 101 (2017) 1-8.

[5] V. Madhu, K. Ramanjaneyulu, T. Balakrishna Bhat, N.K. Gupta, An experimental study of penetration resistance of ceramic armour subjected to projectile impact, International Journal of Impact Engineering. 32 (2005) 337-350.

[6] S.G. Savio, K. Ramanjaneyulu, V. Madhu, T.B. Bhat, An experimental study on ballistic performance of boron carbide tiles, International Journal of Impact Engineering. 38 (2011) 535-541.

[7] Z. Rosenberg, E. Dekel, Terminal Ballistics, Springer, Singapore, 2016.

[8] Wang, C., Xu, W. and Li, T. (2017) “Experimental and numerical studies on penetration of shaped charge into concrete and pebble layered targets”, The International Journal of Multiphysics, 11(3), pp. 295-314.

[9] G.R. Johnson, T.J. Holmquist, A computational constitutive model for brittle materials subjected to large strains, high strain rates and high pressures, in: M.A. Meyers, L.E. Murr, K.P. Staudhammer (éd.), Shockwave and high-strain rate phenomena in materials. Marcel Dekker Inc., New York, USA, 1992

[10] G.R. Johnson, T.J. Holmquist, An improved computational constitutive model for brittle materials, AIP Conference Proceedings. 309 (1994) 981-984.

[11] M.J. Pawar, A. Patnaik, S.K. Biswas, U. Pandel, I.K. Bhat, S. Chatterjee, A.K. Mukhopadhyay, R. Banerjee, B.P. Babu, Comparison of ballistic performances of Al2O3 and AlN ceramics, International Journal of Impact Engineering. 98 (2016) 42-51.

[12] J. Venkatesan, M.A. Iqbal, V. Madhu, Ballistic Performance of Bilayer Alumina/Aluminium and Silicon Carbide/Aluminium Armours, Procedia Engineering. 173 (2017) 671-678.

[13] Mubashar, A., Uddin, E., Anwar, S., Arif, N., Waheed Ul Haq, S., & Chowdhury, M. A. K. (2019). Ballistic response of 12.7 mm armour piercing projectile against perforated armour developed from structural steel. Proceedings of the Institution of Mechanical Engineers, Part L: Journal of Materials: Design and Applications, 233(10), 1993-2005.

[14] Abaqus Analysis User's Manual, Dassault Systemes, Providence, RI, USA, 2014.

[15] N. Kılıç, B. Ekici, Ballistic resistance of high hardness armor steels against 7.62 mm armor piercing ammunition, Materials & Design. 44 (2013) 35-48.

[16] Santos, E. Córdoba, Z. Ramírez, C. Sierra, Y. Ortega, Determination of the coefficient of dynamic friction between coatings of alumina and metallic materials, Journal of Physics: Conf. Series. 935 (2017) 1-6.

[17] A.J. Zukas, Introduction to Hydrocodes, Elsevier Ltd., Netherlands, 2004.

[18] G.R. Johnson, W.H. Cook, Fracture characteristics of three metals subjected to various strains, strain rates, temperatures and pressures, Engineering Fracture Mechanics. 21 (1985) 31-48.

[19] A.H. Clausen, T. Børvik, O.S. Hopperstad, A. Benallal, Flow and fracture characteristics of aluminium alloy AA5083–H116 as function of strain rate, temperature and triaxiality, Materials Science and Engineering: A. 364 (2004) 260-272.

[20] T. Børvik, M.J. Forrestal, O.S. Hopperstad, T.L. Warren, M. Langseth, Perforation of AA5083-H116 aluminium plates with conical-nose steel projectiles – Calculations, International Journal of Impact Engineering. 36 (2009) 426-437.

[21] F. Grytten, T. Børvik, O.S. Hopperstad, M. Langseth, Low velocity perforation of AA5083-H116 aluminium plates, International Journal of Impact Engineering. 36 (2009) 597-610.

[22] M.W. Ali, A. Mubashar, E. Uddin, S.W.U. Haq, M. Khan, An experimental and numerical investigation of the ballistic response of multi-level armour against armour piercing projectiles, International Journal of Impact Engineering. 110 (2017) 47-56.

[23] M. Giglio, A. Gilioli, A. Manes, L. Peroni, M. Scapin, Investigation about the influence of the mechanical properties of lead core and brass jacket of a NATO 7.62 mm ball bullet in numerical simulations of ballistic impacts, DYMAT 2012 - 10th International Conference on the Mechanical and Physical Behaviour of Materials under Dynamic Loading. Freiburg, Germany, 2012 pp. 04010.04011-04015

[24] Gazonas, George A. Implementation of the Johnson-Holmquist II (JH-2) constitutive model into DYNA3D. No. ARL-TR-2699. Army Research Lab Aberdeen Proving Ground MD Weapons and Materials Research Directorate, 2002.

[25] G. McIntosh, The Johnson-Holmquist Ceramic Model as used in LS-DYNA2D. Department of National Defence Canada, 1998
[26] S.C. Duane, K. Bui, C. Kaufmann, G. McIntosh, T. Berstad, Implementation and validation of the Johnson-Holmquist ceramic material model in LS-Dyna, 4th European LS-DYNA User's Conference. Ulm, Germany, 2003 pp. D_I_47-D_I_60
[27] A.I.H. Committee, ASM Handbook Vol 2 - Properties and selection: Nonferrous alloys and special purpose materials, ASM International, Materials Park, OH, USA, 1990.
[28] D.R. Scheffler, Modeling the effect of penetrator nose shape on threshold velocity for thick aluminum targets. Army Research Laboratory, 1997
[29] N. Kılıç, S. Bedir, A. Erdik, B. Ekici, A. Taşdemirci, M. Güden, Ballistic behavior of high hardness perforated armor plates against 7.62mm armor piercing projectile, Materials & Design. 63 (2014) 427-438.
[30] M.A. Iqbal, K. Senthil, P. Sharma, N.K. Gupta, An investigation of the constitutive behavior of Armox 500T steel and armor piercing incendiary projectile material, International Journal of Impact Engineering. 96 (2016) 146-164.
[31] Serjouei, R. Chi, Z. Zhang, I. Sridhar, Experimental validation of BLV model on bi-layer ceramic-metal armor, International Journal of Impact Engineering. 77 (2015) 30-41.